2016 NDIA GROUND VEHICLE SYSTEMS ENGINEERING AND TECHNOLOGY SYMPOSIUM
MODELING & SIMULATION, TESTING AND VALIDATION (MSTV) TECHNICAL SESSION
AUGUST 2-4, 2016 - NOVI, MICHIGAN

USE OF ELECTRIC MACHINE SCALING TECHNIQUES FOR MILITARY VEHICLE POWERTRAIN DESIGN

Yuanying Wang
Heath Hofmann
Department of EECS
University of Michigan
Ann Arbor, MI

Andrej Ivanco
Clemson University
Clemson, SC

Denise Rizzo
TARDEC
Warren, MI

ABSTRACT

With the development of the next generation of military vehicles, the demand for significant amounts of electrical power is increasing, making the design of electrical machines, such as the vehicle alternator, integral to the powertrain design. This shows the importance of the machines' size and efficiency, and the great influence they will have on the vehicle powertrain design process. In this paper, a finite-element-based scaling technique, capable of quickly generating torque-speed curves and efficiency maps for new machine designs, is improved to have two dimensional scaling factors instead of scaling the dimensions uniformly, thus increasing the flexibility of the tool. First, a magnetostatic finite-element-analysis (FEA) is conducted on a base machine, producing data such as torque, flux linkage, and demagnetizing field intensity in the permanent magnets, over a wide range of current magnitudes and phase angles. Then, based on the dimensional and winding scaling factors of the new design, the data is scaled to generate the corresponding torque-speed curves and efficiency maps through post-processing techniques. Finally, the applications of this technique are discussed.

INTRODUCTION

The requirement for large amounts of electric power in military vehicles makes it important for vehicle powertrain designers to have access to models of electric machines that are both accurate and computationally efficient. In previous work [24], a fast way to analyze new designs of electric machines was proposed: first, an appropriate method is used to analyze the electromagnetic behavior of the base electric machine and, second, scaling techniques are applied to quickly predict the performance of new designs. Finite-element-analysis (FEA) is used to analyze the base model. Two types of FEA are widely used in applications: magnetostatic (MS) and magnetoquasistatic (MQS). There is a trade-off between these two methods. The MS FEA method is preferred for its computational efficiency at the cost of accuracy, since it ignores dynamic effects. The MQS FEA method is the opposite: it models the dynamic response, yet is less computationally efficient. Many applications which place emphasis on computational efficiency use MS FEA, as shown in [1-7].

MS FEA-based models are useful in many applications; for instance, [8] and [9] for machine design, [10] for machine control, and [11] for EV/HEV powertrain analysis [24]. References [12-17] indicate that torque-speed curves and efficiency maps of electric machines are of great use in EV/HEV powertrain-level simulation and optimization [24]. However, using FEA to generate the torque-speed curves and efficiency maps can be quite time-consuming. This is validated in [18], in which the generation of an efficiency map for an electric machine takes twelve core-hours. A polynomial model is provided by [19] to avoid using FEA to calculate saturation and cross coupling, and a simplified FEA method for calculating iron loss for salient PM machines is presented.

A method to quickly determine the performance of new designs of electric machines is also essential [24]. References [20-22] proposed and discussed the concept of dimensional scaling, but are limited to parameter changes, thus lacking flexibility. Reference [23] proposed winding and dimensional scaling in the radial and axial directions without considering

the possibility of changing wye-or-delta configurations, or developing accurate methods to obtain efficiency maps and torque-speed curves.

Based on previous work [24], which establishes an FEA-based model of electric machines, and then scales dimensional and winding factors, this paper adds the flexibility of scaling the axial and radial dimensions independently. It allows the designers to propose more possible designs for particular specifications. Using this improved scaling technique, the performance of a machine with similar structure but different scaling can be easily predicted, avoiding the computationally-intensive FEA method. This quick and efficient method can be implemented in the simulation and optimization of the vehicle powertrain and benefit system analysis and design.

This paper will be organized in the following manner. In section II, the MS FEA of previous work is introduced. In section III, the improved dimensional scaling technique, the winding scaling technique of the previous work, and the corresponding relations between the base design and new design are discussed. In section IV, the proposed scaling process is simulated and results are presented. In section V, a military vehicle design procedure using the improved scaling technique is presented. It is important to note that a permanent magnet (PM) machine is used in the case study, though this technique can actually be applied to other types of machines, such as induction machines and synchronous field-winding machines.

FINITE-ELEMENT MODELING AND POST-PROCESSING

A nonlinear 2D magnetostatic finite-element-analysis is used to analyze the base model's electromagnetic performance. The analysis takes the current magnitude, current phase angle, and rotor position as inputs to calculate average torque, flux linkage, and losses, including conduction losses, core losses, and power electronics losses. This was achieved in previous work [24].

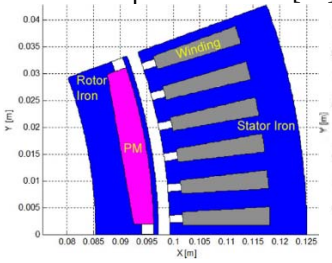

Figure 1. (a)

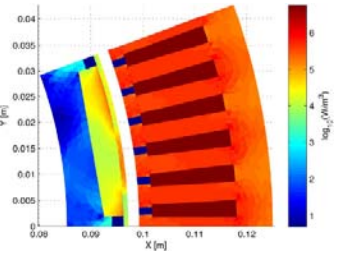

Figure 1. (b)

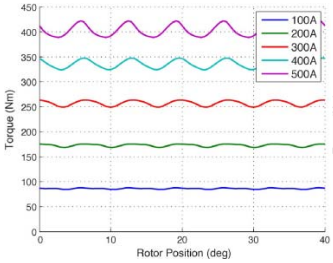

Figure 1. (c)

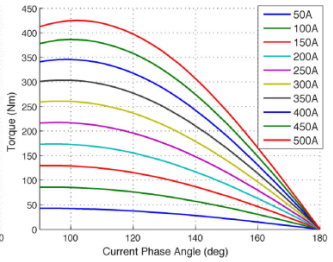

Figure 1. (d)

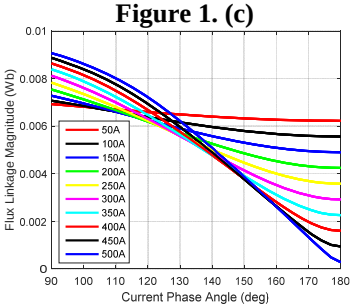

Figure 1. (e)

Figure 1. FEA modeling of the base design [24] ,(a) Two-dimensional geometry of UQM Powerphase 145; (b) Loss distribution at 400 A, 140℃, 4000rpm (logarithmic scale); (c) Torque versus rotor position at different current magnitude when current phase angle is 90°; (d) Torque versus current phase angle at different current magnitudes; (e) Flux linkage magnitude versus current phase angle at different current magnitudes.

Figure 1. (b) shows the power loss density in the machine, as determined by finite element analysis. The winding region has current-dependent copper loss, while the stator iron has core losses, which are generated by time-varying magnetic fields. Core losses are therefore a strong function of frequency, and hence rotor speed. The permanent magnets in the machine have eddy current losses, which are also dependent on the magnetic field and frequency. The rotor iron doesn't have significant core loss, as it is rotating synchronously with the magnetic field provided by the stator winding.

Figure 1. (c) shows the torque as a function of current magnitude and rotor position. It is seen that the torque "ripple" becomes significant at high current levels. The average torque over a rotor revolution is therefore calculated and used to characterize the operating point.

Figure 1. (d) shows the average torque as a function of current magnitude and phase angle. The current angle determines the machine's operating point. For example, as can be seen, the maximum torque for a given current magnitude is achieved when the current angle is a little higher than 90 degrees with respect to the permanent magnet field. This is due to the magnetic saliency of the machine; without

saliency, the torque would maximize exactly at 90 degrees. The maximum torque-per-amp operating point minimizes copper losses. However, the magnetic flux density is high at this operating point, which results in large core loss. Larger current angles result in "field-weakening", shown in Figure 1. (e), which reduces magnetic flux and hence core losses at the expense of higher copper losses for a given torque. For a given torque and speed, there is therefore an optimal current magnitude and phase angle which minimizes the overall loss in the machine. Field weakening is also used to stay within the voltage constraints of the power electronic inverter.

SCALING TECHNIQUES FOR ELECTRIC MACHINES

The database calculated using the FEA model is then scaled by two dimensional scaling factors and one number-of-turns scaling factor, which allows the quick generation of new machine designs. The following sections will detail how the three scaling factors (α, β, δ) can be used to generate the performance of the new design. The first two are the dimensional scaling factors in the radial and axial coordinate directions, respectively, and the third is the winding scaling factor, all of which are clarified in the following.

Dimensional Scaling

Figure 2 shows a cross-section of a conventional surface-mount permanent magnet machine, where the stator surrounds the rotor. The machine volume is decomposed in the axial direction into two parts: the active part and the inactive part. Torque is produced by the active part, whose length is shown in figure 2 as L_{stack}, so-called because it is the length of the laminated stator iron stack. This is the region of the machine where essentially all of the torque is produced. The inactive part consists of 3 lengths: L_{end}, corresponding to the length of the winding "end-turns", $L_{housing}$, corresponding to the axial thickness of the machine housing, and L_{air}, corresponding to the length of the air gap between the end-turns and housing.

As mentioned in the prequel, the stator iron is laminated to minimize eddy currents in the iron. The machine is therefore designed so that the magnetic flux density vector $\vec{B}$ in the iron is constrained to the plane of lamination; i.e., it has no axial component.

$$\vec{B} = B_r(r,\theta)\hat{r} + B_\theta(r,\theta)\hat{\theta} \tag{1}$$

This also holds true for the magnetic field intensity $\vec{H}$, and the magnetization $\vec{M}$ of the material.

$$\vec{H} = H_r(r,\theta)\hat{r} + H_\theta(r,\theta)\hat{\theta} \tag{2}$$

$$\vec{M} = M_r(r,\theta)\hat{r} + M_\theta(r,\theta)\hat{\theta} \tag{3}$$

As a result, the magnetic vector potential $\vec{A}$ in the active region is constrained to the axial direction, and is solely a function of the polar coordinates r and θ.

$$\vec{A} = A(r,\theta)\hat{z} \tag{4}$$

This also holds true for the electric field intensity. As a result, the gradient of electric scalar potential φ in the active region is also limited to the axial direction:

$$\nabla\varphi = \frac{\partial\varphi}{\partial z}\hat{z} \tag{5}$$

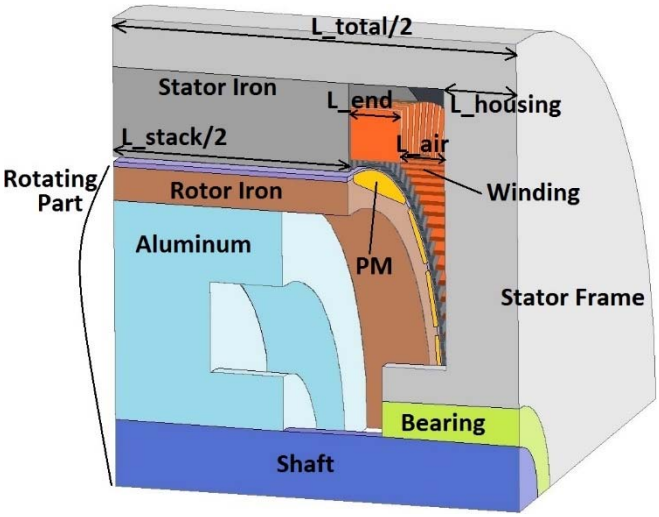

Figure 2. 90 degrees of the studied PM machine (half geometry).

The first scaling method is to scale the polar and the axial coordinate of the base design by factors α and β, respectively, as follows:

$$r_\alpha = \alpha r_1 \tag{6}$$

$$z_\beta = \beta z_1 \tag{7}$$

where r denotes the radial dimension, z denotes the axial dimension, the subscript "1" corresponds to the base design, and the subscript "d" corresponds to the dimensionally-scaled design.

The length of the active part of the scaled machine, which determines its performance, is not scaled by β. This is because the axial length of the housing and air gap between the winding and housing, shown in figure 2, will remain the same as the base design. On the other hand, because the end turns are in polar coordinates which are scaled by α, so the length of the end turns will also be scaled by α. Thus, the scaling factor of the active length l_{stack} is therefore:

$$L_{stack,d} = \gamma L_{stack,1}, \tag{8}$$

where $\gamma = \frac{\beta L_{total,1} - 2\alpha L_{end,1} - 2L_{air,1} - 2L_{housing,1}}{L_{total,1} - 2L_{end,1} - 2L_{air,1} - 2L_{housing,1}}$.

When deriving the new scaling techniques, we will use different expressions for the scaling of differential operators in polar and axial coordinates. For polar coordinates, we have:

$$\nabla_\alpha = \frac{1}{\alpha}\nabla_1 \tag{9}$$

$$\nabla_\alpha^2 = \frac{1}{\alpha^2}\nabla_1^2 \tag{10}$$

Whereas for the axial direction we will have:

$$\frac{\partial}{\partial z_\gamma} = \frac{1}{\gamma}\frac{\partial}{\partial z_1} \tag{11}$$

In the scaled design, the magnetic flux density $\vec{B}$ and magnetic field intensity $\vec{H}$ are mandated to remain consistent with the base design:

$$\vec{B}_d(r_\alpha, \theta) = \vec{B}_1(r_1, \theta) \tag{12}$$

$$\vec{H}_d(r_\alpha, \theta) = \vec{H}_1(r_1, \theta) \tag{13}$$

The scaled material magnetization is therefore:

$$\vec{M}_d(r_\alpha, \theta) = \vec{M}_1(r_1, \theta) \tag{14}$$

Since the magnetic flux density is kept consistent:

$$\begin{aligned}\vec{B}_d &= \nabla_\alpha \times (A_d\hat{z}) = \vec{B}_1 = \nabla_1 \times (A_1\hat{z}) \\ &= \frac{1}{\alpha}\nabla_1 \times (A_d\hat{z}) = \nabla_1 \times \left(\frac{1}{\alpha}A_d\hat{z}\right)\end{aligned} \tag{15}$$

The scaled magnetic vector potential relationship is therefore:

$$A_d(r_\alpha, \theta) = \alpha A_1(r_1, \theta) \tag{16}$$

The steady electromagnetic dynamics reveals that [21]:

$$\frac{1}{\mu_o}\nabla_1^2 A_1 - \sigma\frac{\partial}{\partial z_1}\varphi_1 - \sigma\frac{\partial A_1}{\partial t_1} + \nabla_1 \times \vec{M}_1 = 0 \tag{17}$$

$$\frac{1}{\mu_o}\nabla_\alpha^2 A_d - \sigma\frac{\partial}{\partial z_\gamma}\varphi_d - \sigma\frac{\partial A_d}{\partial t_d} + \nabla_\alpha \times \vec{M}_d = 0 \tag{18}$$

So, based on equations (9)-(11) and (16), equation (18) changes to:

$$\frac{1}{\alpha}\frac{1}{\mu_o}\nabla_1^2 A_1 - \sigma\frac{1}{\gamma}\frac{\partial}{\partial z_1}\varphi_d - \sigma\frac{\partial \alpha A_1}{\partial t_d} + \frac{1}{\alpha}\nabla_1 \times \vec{M}_d = 0 \tag{19}$$

Equation (19) multiplied by α is:

$$\frac{1}{\mu_o}\nabla_1^2 A_1 - \sigma\frac{\alpha}{\gamma}\frac{\partial}{\partial z_1}\varphi_d - \sigma\alpha^2\frac{\partial A_1}{\partial t_d} + \nabla_1 \times \vec{M}_d = 0 \tag{20}$$

Comparing equation (20) with equation (17), the scaling relationships between the electric potential φ and time t are set as follows:

$$\varphi_d = \frac{\gamma}{\alpha}\varphi_1 \tag{21}$$

$$t_d = \alpha^2 t_1 \tag{22}$$

The temporal scaling provides a scaling for rotor angular velocity:

$$\omega_d = \frac{1}{\alpha^2}\omega_1 \tag{23}$$

The electric field scaling relationship is:

$$\begin{aligned}E_d &= -\frac{\partial}{\partial z_\gamma}\varphi_d - \frac{\partial A_d}{\partial t_d} \\ &= -\frac{1}{\gamma}\frac{\partial}{\partial z_1}\left(\frac{\gamma}{\alpha}\varphi_1\right) - \frac{1}{\alpha}\frac{\partial A_1}{\partial t_1} = \frac{1}{\alpha}E_1\end{aligned} \tag{24}$$

So the scaled current density is therefore given by:

$$J_d = \sigma E_d = \frac{1}{\alpha}\sigma E_1 = \frac{1}{\alpha}J_1 \tag{25}$$

The winding area S in the polar coordinates and the active winding length L along the axial coordinates are scaled as follows:

$$S_\alpha = \alpha^2 S_1 \tag{26}$$

$$L_\gamma = \gamma L_1 \tag{27}$$

The scaled current and winding are given by:

$$I_d = S_\alpha J_d = \alpha I_1 \tag{28}$$

$$R_d = \sigma\frac{L_\gamma}{S_\alpha{}^2} = \frac{\gamma}{\alpha^2}R_1 \tag{29}$$

The flux linkage is then given by:

$$\lambda_d = A_d \cdot L_\gamma = \alpha\gamma\lambda_1 \tag{30}$$

And the terminal voltage is therefore:

$$V_d = R_d I_d + \frac{d\lambda_d}{dt_d} = \frac{\gamma}{\alpha^2}\alpha R_1 I_1 + \frac{\alpha\gamma}{\alpha^2}\frac{d\lambda_1}{dt_1} = \frac{\gamma}{\alpha}V_1 \tag{31}$$

The Maxwell stress tensor given in Cartesian coordinates is:

$$\vec{T}_d = \frac{1}{\mu_o}\begin{bmatrix} B_x^2 - \frac{\|\vec{B}\|^2}{2} & B_xB_y & B_xB_z \\ B_yB_x & B_y^2 - \frac{\|\vec{B}\|^2}{2} & B_yB_z \\ B_zB_x & B_zB_y & B_z^2 - \frac{\|\vec{B}\|^2}{2} \end{bmatrix} = \vec{T}_1 \quad (32)$$

So the scaled torque can then be represented as:

$$\tau_{em,d} = \oint \vec{r_\alpha} \times T_d \vec{d} S_d = \alpha^2\gamma \oint \vec{r_1} \times T_1 \vec{d} S_1 = \alpha^2\gamma\tau_{em,1} \quad (33)$$

Based on equation (25) the conduction power loss density relationship is given by:

$$q_{c,d} = \frac{1}{\alpha^2} q_{c,1} \quad (34)$$

The hysteresis loss density relationship is:

$$q_{h,d} = f_d \oint \vec{H}_d \, d\vec{B}_d = \frac{1}{\alpha^2} f_1 \oint \vec{H}_1 \, d\vec{B}_1 = \frac{1}{\alpha^2} q_{h,1} \quad (35)$$

So the total power loss is thus given by:

$$P_{loss,d} = \oint (q_{c,d} + q_{h,d}) \, d\mathcal{V}_d = \frac{1}{\alpha^2} \oint (q_{c,1} + q_{h,1}) \, d\alpha^2\gamma\mathcal{V}_1 = \gamma P_{loss,1} \quad (36)$$

where $\mathcal{V}$ denotes the volume unit of the machine.

The scaled mechanical power is therefore given by:

$$P_{mech,d} = \omega_d \tau_{em,d} = \gamma P_{mech,1} \quad (37)$$

Using (23), (33), (36) and (37), and the base design information, the torque-speed curve and the efficiency map of the new scaled design can be directly generated.

Winding Scaling

The second scaling method is to scale the effective number of turns in the winding.

The effective number of turns is used to determine the total flux linkage linking one phase [24]. It will influence the terminal voltage-current relationship, which is mainly affected by three factors: the actual number of turns per coil, the number of parallel paths, and whether the machine windings are in wye or delta configuration. The number of parallel paths indicates the structure of the winding of one phase. For example, the winding scaling can be calculated using equation (36) which was done in previous work [24], by choosing the three factors as follows; 1) the number of turns per coil can be chosen to be any natural number; 2) the number of parallel paths can be chosen to be any divisor of P/2, where P is the number of poles (18 in our example) ;3) $YorDelta$ can be either 1 (for wye winding configuration) or $1/\sqrt{3}$ (for delta configuration) [24]:

$$\text{Number of turns scaling: } N_{sc,t} = \delta \times N_1 \quad (38)$$

$$\text{Voltage: } V_{sc,t} = \delta \times V_1 \quad (39)$$

where $\delta = \frac{nTurns_t}{nPP_t} / \frac{nTurns_1}{nPP_1} \times \frac{YorDelta_t}{YorDelta_1}$, the subscript "1" for the base design, and the subscript "t" for the winding scaled design. In conclusion, the scaled machine design can be easily generated from the pre-calculated FEA model and three scaling factors (α, β, δ), while avoiding computationally-intensive FEA for every new machine design.

SIMULATION AND RESULTS

The procedure of predicting performance for a new scaled machine design can be divided into three parts: 1) the generation of the base FEA model and the calculation of the base model database; 2) the choice of the scaling factors and the generation of the scaled design; 3) the generation of the torque-speed curve and the efficiency map for the new scaled designs.

Figure 4 shows the comparison between the efficiency maps of a scaled SMPM and different scaling factors, with the base design.

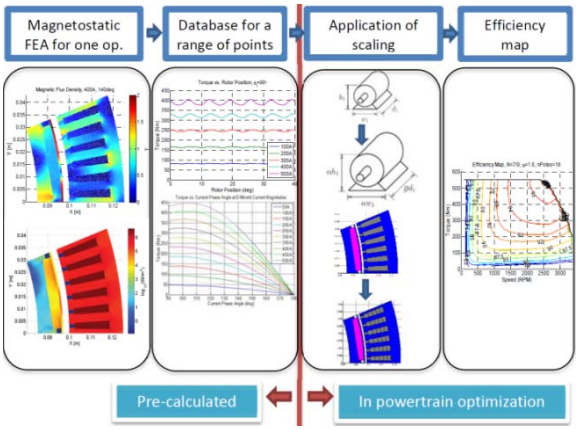

Figure 3. Electric machine Scaling and Efficiency Map Generation [24]

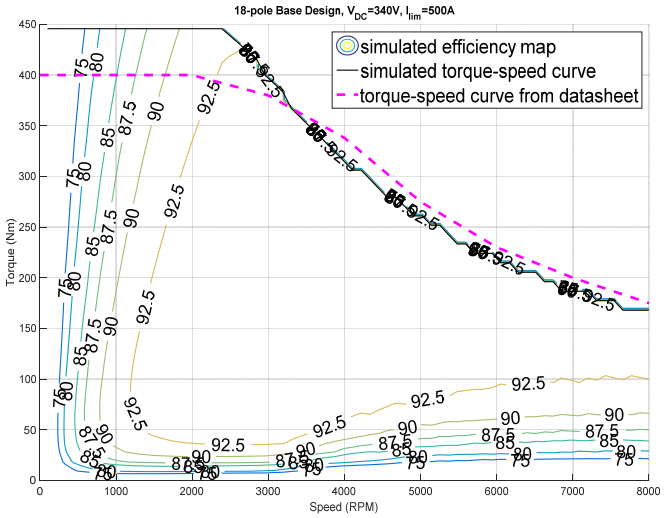

Figure 4. (a) Base design

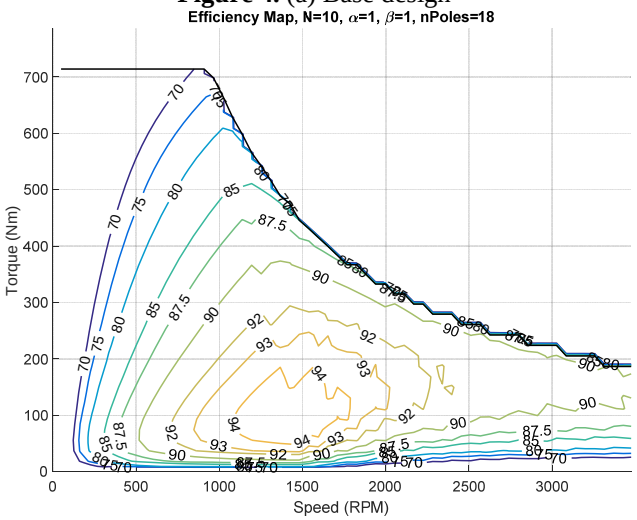

Figure 4. (b)

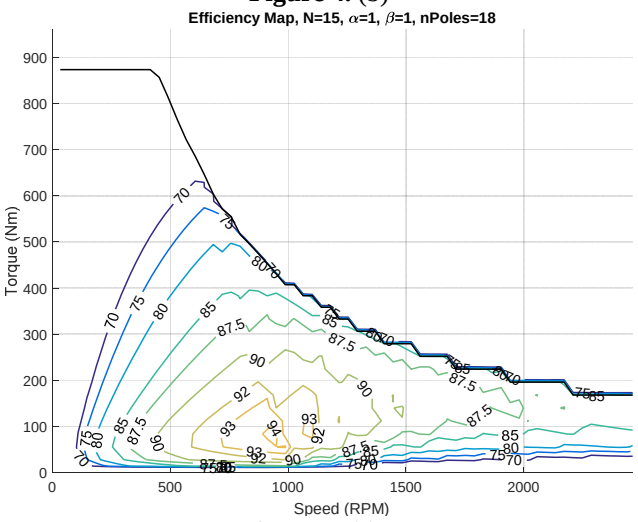

Figure 4. (c)

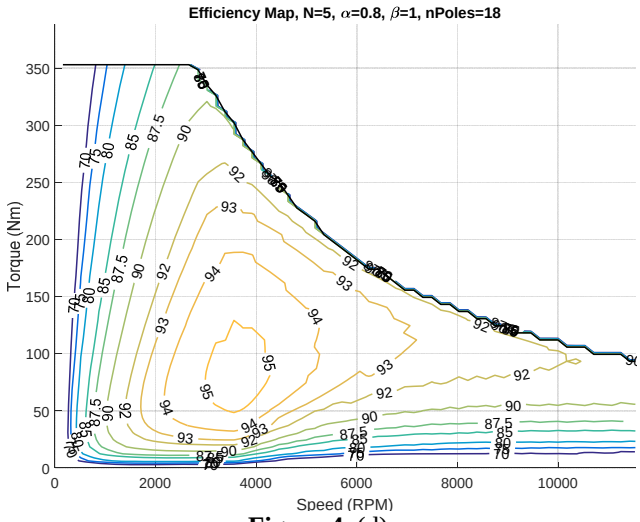

Figure 4. (d)

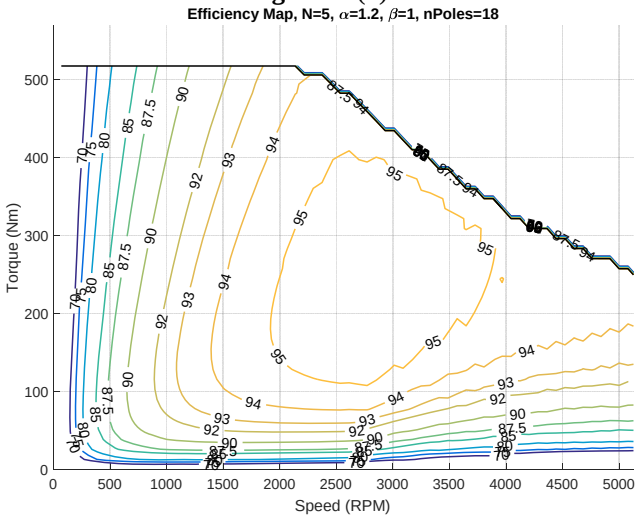

Figure 4. (e)

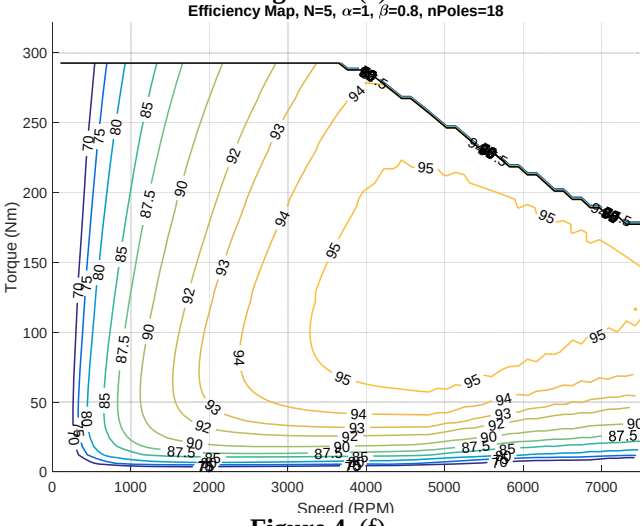

Figure 4. (f)

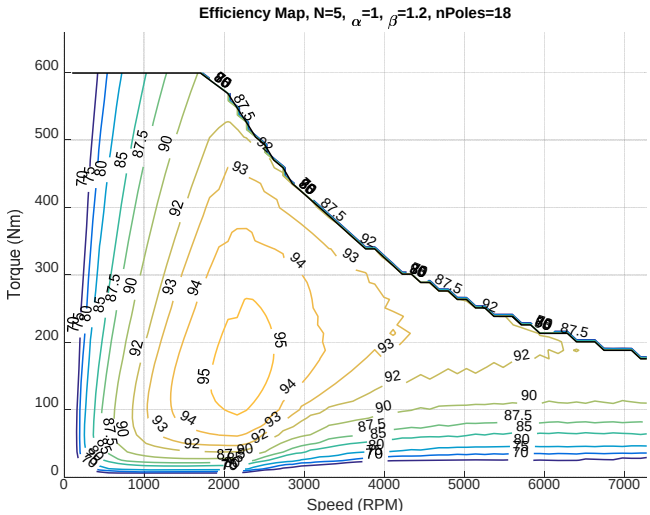

Figure 4. (g)

Figure 4. Comparison between the efficiency maps of a SMPM machine: (a) Base design with $\alpha = \beta = 1, N = 5$; (b) & (c) Number-of-turn scaling with $N = 10$ and $N = 15$, respectively, and $\alpha = \beta = 1$; (d) & (e) Radius scaling with $\alpha = 0.8$ and $\alpha = 1.2$, respectively and $\beta = 1, N = 5$; (f) & (g) Axis scaling with $\beta = 0.8$ and $\beta = 1.2$, respectively, and $\beta = 1, N = 5$.

From the trends shown in figure 4 (a), (b) & (c), it is seen that increasing the number of turns will move the "sweet spot"; i.e., the operating point with maximum efficiency, to lower rotor speed and torque. Another fact to notice is the low efficiency when the rotor speed is low and the torque is large—these operating points may not be feasible due to thermal concerns. The characteristics of figure 4 (a), (d) & (e) demonstrates that increasing the radius will increase the torque to achieve maximum power while the sweet spot moves to a larger rotor speed and torque. The changes shown in figure 4 (a), (f) & (g) illustrate that increasing the axial coordinates will increase the torque under maximum power and the sweet spot moves to lower rotor speed and torque. Adjusting the location of the sweet spot of a machine design, in addition with other powertrain design variables, can optimize the vehicle performance for a given drive cycle, as will be discussed in the next section.

APPLICATIONS

Next, a case study is developed in order to demonstrate the proposed methodology for electric machine design. The objective is to find the right generator design to be coupled to an existing combustion engine to form a "Powerpack" unit. Powerpack is the main onboard energy source in a series-configured hybrid-electric powertrain. Its design is limited by power output capability, where it should provide enough power to satisfy vehicle propulsion requirements but at the same time be light, compact, and operate at the best possible efficiency.

An embedded optimization routine is executed to study the sensitivity of the generator design in a Powerpack configuration with regards to vehicle fuel consumption. A notional medium duty series hybrid electric vehicle configuration with in-wheel motors was selected to demonstrate the fuel consumption variations. The vehicle parameters are summarized in Table 1.

Table 1: Notional vehicle parameters

Vehicle weight	14 ton
In wheel motor power	4x128 kW [26]
Powerpack output	~250 kW electrical
Battery pack	9 kWh

As the Powerpack is mechanically disconnected from the wheels, it can be operated independently from the propulsion power demand and the excess or lack of immediate electrical power can be provided from the battery pack. This solution adds an additional degree of complexity in controls, but offers exceptional mobility as each wheel can be operated independently. Also the hull design can be more flexible, due to the absence of a driveshaft. Finally, the series-configuration can power the vehicle's on-board electrical network as well as act as a stationary generator.

Once the generator design is created, it is used in the vehicle model to evaluate fuel consumption. An embedded configuration benchmark algorithm [25] is used to find the minimum fuel consumption for a given configuration. Then a Matlab genetic algorithm from the global optimization toolbox [27] is used to iterate over possible designs and find the global minimum of fuel consumption, given the flexibility of the generator design.

Figure 5 shows the simulation result of the design optimization. Five major design parameters are compared with respect to the fuel consumption. From top of the Figure 5: The radial and axis scaling factors converge to their respective optimum with values 1.79 and 1.08, respectively. The third parameter in Figure 5, the number of turns, reaches its maximum for number 15, which was the limitation of the design space. The fourth parameter, the number of parallel paths, maximizes the fuel economy at its highest value of 9, which is the allowable maximum for an 18-pole electric machine. The last parameter, wye or delta configuration, is obvious to be better in the "Y" configuration. The overall best fuel economy is reached at 33.5 L/100km, with a range of over 2 L / 100 km, depending on the electric machine design.

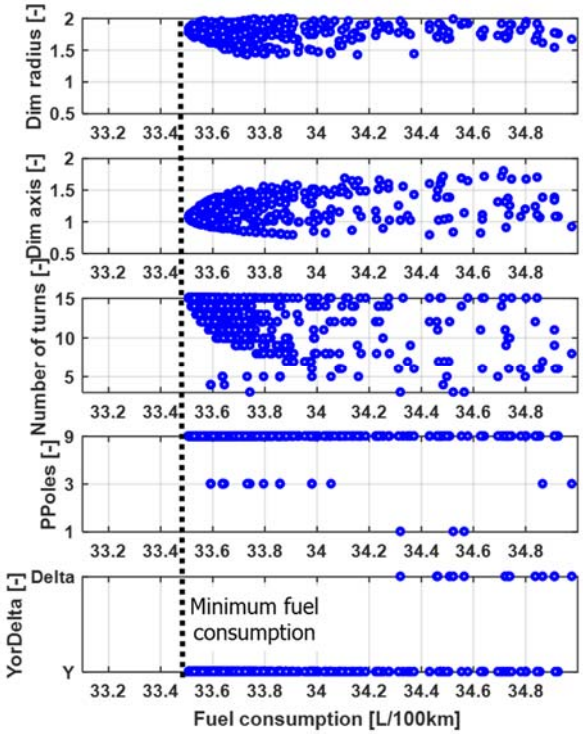

Figure 5. Preliminary optimization results. From top down, respectively: radial and axial scaling, number of winding turns, parallel path scaling, wye-or-delta configurations

Figure 6 depicts the combined efficiency of the engine and the optimized generator, forming a Powerpack. As the Powerpack is mechanically disconnected from the wheels, it can be operated freely along the best efficiency line, constrained only by the desired electrical power output. The rated power for the engine and generator is 255 kW and 256 kW, respectively. The Powerpack should have the power capacity to fulfill the majority of the power demands from the drive cycle, while the battery can balance out the peak load. Based on Figure 6, a few observations can be made about the Powerpack operation as the green box shows the percentage of fuel used during the drive cycle:

- A majority of the fuel is consumed in the most efficient region, right in the middle of the map.
- Only about 1% of fuel is used to satisfy the peak power demand.
- An additional 15% of fuel can be saved if an engine stop-and -function is enabled as the engine is kept idling in the simulation, considering the need for an immediate power response.

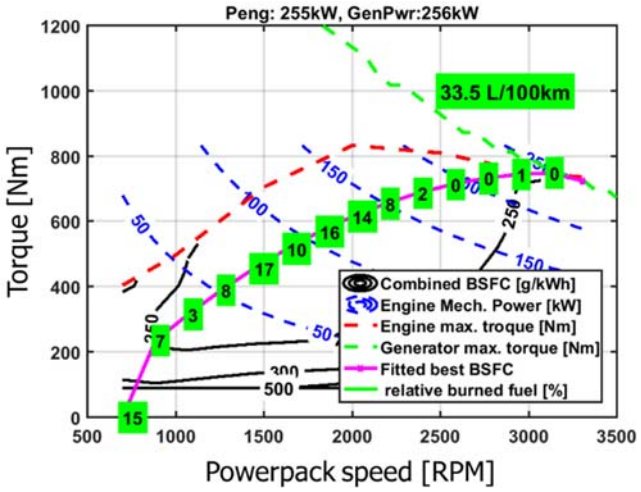

Figure 6. Combined efficiency map for the Powerpack. Numbers in green box represent percent of total fuel consumed at particular operating point

In brief, the new design methodology was validated and an optimized generator design constructed. This will serve as a basis for future work where even more parameters are included into the design optimization routine to find a custom-fit design which minimizes the fuel consumption of military vehicles

CONCLUSIONS

In this paper, an electric machine scaling technique, initially proposed in previous work, has been improved. In the new technique, the radial and axial dimensions of the machine are scaled separately. This increases the flexibility of scaling, so that the designer can come up with more possible designs with particular specifications. Efficiency maps of machine designs with different scaling factors are shown.

The optimization of a PM machine used as a generator in a notional medium-duty military vehicle is demonstrated using the improved scaling techniques. The combined efficiency map and the preliminary optimized fuel consumption are shown.

Future work includes: 1) the integration of a scalable thermal FEA model so as to better estimate the losses depending on temperature; 2) better estimation of ac resistance as a function of electrical frequency; 3) electric machine design sensitivity on different drive cycles.

REFERENCES

[1] D. Ionel, M. Popescu, M. McGilp, T. Miller, and S. Dellinger, "Assessment of torque components in brushless permanent-magnet machines through numerical analysis of the electromagnetic field," *IEEE Trans. Ind. Appl.*, vol. 41, no. 5, pp. 1149–1158, Sep./Oct. 2005.

[2] M. Barcaro, N. Bianchi, and F. Magnussen, "Average and oscillating torque determination in fractional-slot PM motors," in *Proc. 19th ICEM*,Sep. 2010, pp. 1–7.

[3] D. Ionel and M. Popescu, "Finite-element surrogate model for electric machines with revolving field—Application to IPM motors," *IEEE Trans.Ind. Appl.*, vol. 46, no. 6, pp. 2424–2433, Nov./Dec. 2010.

[4] D. Ionel and M. Popescu, "Ultrafast finite-element analysis of brushless PM machines based on space-time transformations," *IEEE Trans. Ind. Appl.*, vol. 47, no. 2, pp. 744–753, Mar./Apr. 2011.

[5] G. Sizov, D. Ionel, and N. Demerdash, "Modeling and parametric design of permanent-magnet AC machines using computationally efficient finite-element analysis," *IEEE Trans. Ind. Electron.*, vol. 59, no. 6, pp. 2403–2413, Jun. 2012.

[6] P. Zhang, G. Sizov, J. He, D. Ionel, and N. Demerdash, "Calculation of magnet losses in concentrated-winding permanent-magnet synchronous machines using a computationally efficient finite-element method," *IEEE Trans. Ind. Appl.*, vol. 49, no. 6, pp. 2524–2532, Nov./Dec. 2013.

[7] T. Miller *et al.*, "Embedded finite-element solver for computation of brushless permanent-magnet motors," *IEEE Trans. Ind. Appl.*, vol. 44, no. 4, pp. 1124–1133, Jul./Aug. 2008.

[8] F. Marignetti, V. Delli Colli, and Y. Coia, "Design of axial flux pm synchronous machines through 3-D coupled electromagnetic thermal and fluid-dynamical finite-element analysis," *IEEE Trans. Ind. Electron.*, vol. 55, no. 10, pp. 3591–3601, Oct. 2008.

[9] R. Wrobel, J. Goss, A. Mlot, and P. Mellor, "Design considerations of a brushless open-slot radial-flux PM hub motor," *IEEE Trans. Ind. Appl.*, vol. 50, no. 3, pp. 1757–1767, May/Jun. 2014.

[10] L. Alberti, N. Bianchi, M. Morandin, and J. Gyselinck, "Finite-element analysis of electrical machines for sensorless drives with signal injection," in *Proc. IEEE ECCE*, Sep. 2012, pp. 861–868.

[11] V. Ruuskanen, J. Nerg, J. Pyrhonen, S. Ruotsalainen, and R. Kennel, "Drive cycle analysis of a permanent magnet traction motor based on magnetostatic finite element analysis," *IEEE Trans. Veh. Technol.*, vol. 64, no. 3, pp. 1249–1254, Mar. 2015.

[12] S. Lukic and A. Emadi, "Modeling of electric machines for automotive applications using efficiency maps," in *Proc. Elect. Insul. Conf. Elect. Manuf. Coil Winding Technol. Conf.*, Sep. 2003, pp. 543–550.

[13] S. Lukic and A. Emadi, "Effects of drivetrain hybridization on fuel economy and dynamic performance of parallel hybrid electric vehicles," *IEEE Trans. Veh. Technol.*, vol. 53, no. 2, pp. 385–389, Mar. 2004.

[14] S. Williamson, M. Lukic, and A. Emadi, "Comprehensive drive train efficiency analysis of hybrid electric and fuel cell vehicles based on motor controller efficiency modeling," *IEEE Trans. Power Electron.*, vol. 21,no. 3, pp. 730–740, May 2006.

[15] J. Estima and A. Marques Cardoso, "Efficiency analysis of drive train topologies applied to electric/hybrid vehicles," *IEEE Trans. Veh. Technol.*,vol. 61, no. 3, pp. 1021–1031, Mar. 2012.

[16] X. Liu *et al.*, "Efficiency improvement of switched flux PM memory machine over interior PM machine for EV/HEV applications," *IEEE Trans. Magn.*, vol. 50, no. 11, Nov. 2014, Art ID. 8202104.

[17] K. Kiyota, H. Sugimoto, and A. Chiba, "Comparison of energy consumption of SRM and IPMSM in automotive driving schedules," in *Proc. IEEE ECCE*, Sep. 2012, pp. 853–860.

[18] E. Dlala *et al.*, "Efficiency map simulations for an interior pm motor with experimental comparison and investigation of magnet size reduction," in *Proc. IEEE IEMDC*, May 2013, pp. 23–29.

[19] J. Goss, P. H. Mellor, R. Wrobel, D.A. Staton, M.Popescu, "The Design of AC Permanent Magnet Motors for electric Vehicles: A Computationally Efficient Model of the Operational Envelope", The Institution of Engineering & Technology, vol 2012.

[20] K.-T. Hsieh and B. Kim, "One kind of scaling relations on electromechanical systems," *IEEE Trans. Magn.*, vol. 33, no. 1, pp. 240–244, Jan. 1997.

[21] J. Pries and H. Hofmann, "Magnetic and thermal scaling of electric machines," *Int. J. Veh. Des.*, vol. 61, no. 1, pp. 219–232, 2013.

[22] K. Upendra and A. Grauers, "Requirements on electric machines for road vehicles—A preliminary study with focus on thermal limits under transient load," Swedish Hybrid Veh. Centre, Chalmers Univ. Technol., Göteborg, Sweden, Tech. Rep., May 2014.

[23] Stjepan Stipetic, Damir Zarko and Mircea Popescu, "Scaling Laws for Synchronous Permanent Magnet Machines," 2015 Tenth International Conference on Ecological Vehicles and Renewable Energies, pp.1-7, June 2015.

[24] Kan Zhou, Andrej Ivanco, Zoran Filipi, and Heath Hofmann, "Finite-Element-Based Computationally Efficient Scalable Electric Machine Model Suitable for Electrified Powertrain Simulation and Optimization," IEEE Trans. Ind. Appl., vol. 51, NO. 6, pp.4435-4444, Nov/Dec. 2015.

[25] A. Ivanco, K. Zhou, H. Hofmann, and Z.S. Filipi, Powerpack Optimal Design Methodology with Embedded Configuration Benchmarking. SAE Int. J. Alt. Power., 2016. 5(2).